

# An Analytical and AI-discovered Stable, Accurate, and Generalizable Subgrid-scale Closure for Geophysical Turbulence

Karan Jakhar,<sup>1,2</sup> Yifei Guan,<sup>1,3</sup> and Pedram Hassanzadeh<sup>4</sup>

<sup>1</sup>*Department of Geophysical Sciences, University of Chicago*

<sup>2</sup>*Department of Mechanical Engineering, Rice University*

<sup>3</sup>*Department of Mechanical Engineering, Union College*

<sup>4</sup>*Department of Geophysical Sciences and Committee on Computational and Applied Mathematics, University of Chicago\**

(Dated: January 5, 2026)

By combining AI and fluid physics, we discover a closed-form closure for 2D turbulence from small direct numerical simulation (DNS) data. Large-eddy simulation (LES) with this closure is accurate and stable, reproducing DNS statistics including those of extremes. We also show that the new closure could be derived from a 4th-order truncated Taylor expansion. Prior analytical and AI-based work only found the 2nd-order expansion, which led to unstable LES. The additional terms emerge only when inter-scale energy transfer is considered alongside standard reconstruction criterion in the sparse-equation discovery.

Subgrid-scale (SGS) closures, or parameterizations, are essential for simulating real-world systems involving turbulent flows [1, 2]. A prominent example is climate modeling, where closures are required for simulating the geophysical turbulence in the atmosphere and ocean, along with various other nonlinear, multi-scale processes [3–5]. Despite over a century of research, a general framework for deriving turbulence closures from first principles has remained elusive, resulting in the widespread reliance on semi-empirical and ad-hoc models [2, 6, 7]. In fact, the shortcomings of these closures are the main source of epistemic uncertainty in climate change projections and weather forecasts, especially for extreme events [8–11]. This has led to extensive efforts in recent decades to pursue innovative physical, mathematical, and, recently, artificial intelligence (AI) tools to develop SGS closures for geophysical flows [11–14].

An ideal closure 1) should accurately capture the detailed structure of the SGS fluxes, 2) should accurately reproduce the interactions between the SGS processes and the resolved, large-scale dynamics, e.g., the inter-scale energy and enstrophy transfers, and 3) when coupled to the numerical solver of the resolved scales, e.g., in large-eddy simulation (LES), the simulated flow should have key characteristics such as energy and enstrophy spectra matching those of the direct numerical simulation (DNS). In the context of weather and climate prediction, of particular interest is also capturing the statistics of rare (extreme) events. *However, currently, a framework for developing closures satisfying (1)–(3) is lacking* [1, 2, 6].

The “structural modeling” approach [2], e.g., based on truncated Taylor-series expansion of the SGS flux, yields closures such as the nonlinear gradient model (NGM2), which satisfies (1) with above 0.9 pattern correlation with filtered DNS (FDNS) [15–17]. However, these closures fail (2)–(3), e.g., producing no inter-scale energy trans-

fer in 2D turbulence and leading to unstable LES [18–21]. The “functional modeling” approach [22–25] leads to eddy-viscosity closures such as Smagorinsky [26] and Leith [25], which produce stable LES and some aspects of (2) though they are often overly dissipative and miss backscattering (the transfer of energy from the SGS processes to the resolved scales), an important process in atmospheric and oceanic flows [4, 27–36]. Excessive dissipation also degrades the representation of extreme events [37, 38]. Furthermore, these closures fail (1), e.g., lower than 0.5 pattern correlation [37, 39, 40].

Recently, AI approaches for developing data-driven closures have received significant attention. Most efforts have focused on supervised learning with FDNS data, which is an approach akin to structural modeling [7, 11, 41, 42]. While some studies have demonstrated that these data-driven closures can satisfy conditions (1)–(3), they suffer from three major limitations: (i) the need for large amounts of DNS snapshots for training, (ii) lack of interpretability, and (iii) poor generalization to out-of-distribution regimes, e.g., extrapolation to much higher Reynolds numbers [37, 43–46]. Other AI frameworks have also shown success, including self-supervised approaches, akin to functional modeling, which use only DNS statistics, and those that directly learn the coarse-grained dynamics [47–50]. However, these approaches can still suffer from shortcomings (ii) and (iii).

A number of studies have pursued an alternative approach: “equation discovery”, a class of AI techniques that aim to find a closed-form mathematical representation of the data [51–58]. The major appeals of this approach are data efficiency, interpretability, and generalizability, thus addressing the shortcomings of deep learning. In their pioneering work, Zanna and Bolton [20] used Bayesian sparse regression to find a closed-form equation for SGS momentum stress in geophysical turbulence. They robustly discovered a closure that resembled NGM2 but found that while this closure accurately captured the detailed structure of the SGS fluxes, the LES was unstable (unless the predicted SGS flux was attenuated).

\* [pedramh@uchicago.edu](mailto:pedramh@uchicago.edu)

Using the same methodology, [21] discovered closures of the same structure for SGS momentum and heat fluxes across various setups of 2D turbulence and Rayleigh-Bénard convection and confirmed that they all exactly match the outcome of second-order truncated Taylor-series expansion; i.e., the discovered closure is NGM2. They also demonstrated that the LES instability results from NGM2's inability to capture any inter-scale energy transfer (neither diffusion nor backscattering). However, it remained unclear how a better equation discovery approach can be devised, though the need for a physics-informed loss function and a better library (e.g., through genetic programming [33, 51]) was speculated.

In this Letter, we inform the criterion for “discovery” of a sparse representation with the fundamental understanding of turbulence physics. We robustly find, for diverse setups of 2D turbulent flows and with an expansive library, a closure that is NGM2 plus an additional term. We further show that this additional term is, in fact, the 4th-order term in the Taylor-series expansion of the SGS flux. We demonstrate that this new closure (NGM4, hereafter), accurately captures the structure of the SGS flux (pattern correlation  $\approx 0.99$ ), accurately reproduces the inter-scale energy and enstrophy transfers, and leads to stable LES, that among other things, accurately reproduces the statistics of the rare, extreme events in diverse test cases that cover a broad range of dynamics mimicking atmospheric and oceanic turbulence.

The dimensionless continuity and momentum equations for LES of 2D turbulence are given by:

$$\frac{\partial \bar{u}_i}{\partial x_i} = 0, \quad (1)$$

$$\frac{\partial \bar{u}_i}{\partial t} + \frac{\partial \bar{u}_i \bar{u}_j}{\partial x_j} = -\frac{\partial \bar{p}}{\partial x_i} + \frac{1}{Re} \frac{\partial^2 \bar{u}_i}{\partial x_j \partial x_j} - \frac{\partial \tau_{ij}}{\partial x_j} + \bar{Q}_i. \quad (2)$$

Here,  $\bar{(.)}$  represents a low-pass filtering operation,  $u_i$  denotes velocity,  $p$  is pressure,  $Re$  is the Reynolds number, and  $\bar{Q}_i$  represents a time-invariant external forcing, Rayleigh drag, and the Coriolis force. The SGS stress tensor,  $\tau_{ij} = \bar{u}_i \bar{u}_j - \bar{u}_i \bar{u}_j$ , requires a closure model that expresses  $\tau_{11}, \tau_{12} = \tau_{21}$ , and  $\tau_{22}$ , as a function of the resolved flow variables  $(\bar{u}_i, \bar{p})$ .

We investigate four cases of 2D turbulence, generating a diverse flow dynamics that vary in dominant length scales and energy ( $E = \frac{1}{2} u_i u_i$ ) and enstrophy ( $Z = \frac{1}{2} \omega^2$ ) cascade regimes ( $\omega$  is the vorticity); see Appendix A for more information about these cases and their properties. Here, we regard direct numerical simulation (DNS) data as the ground truth (details of the numerical solvers are in Appendix C). We utilize FDNS data to learn closure for  $\tau_{ij}$ . The FDNS data are obtained by first filtering the DNS data using a Gaussian filter and then coarse-graining the results to the 4 to 64 $\times$  coarser LES grid following Jakhar *et al.* [21]. The equation discovery method used in this study is a sparsity-promoting Bayesian linear regression approach [20, 54, 59] based on the relevance vector machine (RVM) [60], employed to derive closed-form closures for each element of  $\tau_{ij}$  using FDNS data.

This method operates on a library of basis functions,  $\Phi$ , comprising linear or nonlinear combinations of relevant variables, such as velocity or its derivatives:

$$\left[ \frac{\partial^{(q_1+q_2)} A}{\partial x^{q_1} \partial y^{q_2}} \right]^{p_1} \left[ \frac{\partial^{(q_4+q_5)} B}{\partial x^{q_4} \partial y^{q_5}} \right]^{p_2} \left[ \frac{DC}{Dt} \right]^{p_3}, \quad (3)$$

where  $A, B = \bar{u}_1$  and  $\bar{u}_2$ ,  $(x, y) = (x_1, x_2)$ , and  $C = \bar{\omega}$  or an element of  $\bar{S}_{ij} = \frac{1}{2} \left( \frac{\partial \bar{u}_i}{\partial x_j} + \frac{\partial \bar{u}_j}{\partial x_i} \right)$ , the strain rate. Material derivative  $\frac{D}{Dt} = \frac{\partial}{\partial t} + u_j \frac{\partial}{\partial x_j}$  is included to account for non-Markovian (memory) effects, motivated by Mori-Zwanzig formalism [61, 62].

This library is extensive, with integers  $0 \leq q \leq 8$  and  $0 \leq p \leq 2$ , although the total derivative order is constrained to 8th (yielding a total of 930 terms in the library). To accurately compute higher-order spatial derivatives required for this study, we used arbitrary-precision methods [63]. The construction of this library is motivated by the Galilean-invariant and symmetry properties of the SGS terms; e.g., this library includes the Pope's tensors [33, 64–70].

The library must be comprehensive enough to express  $\mathbf{s}$ , a vectorized element of  $\tau_{ij}$ , as  $\mathbf{s}^{\text{RVM}} = \Phi \mathbf{c}$ . The regression weights,  $\mathbf{c}$ , are optimized by minimizing the error  $\text{MSE} = \|S^{\text{RVM}} - S^{\text{FDNS}}\|_2^2$ , where  $S$  consists of  $n$  stacked samples of  $\mathbf{s}$ . The RVM enforces sparsity by iteratively pruning basis functions with weights exhibiting uncertainties above a predefined threshold,  $\alpha$ , and recalculating the MSE until all remaining functions have uncertainties below  $\alpha$ . A higher  $\alpha$  increases model complexity but reduces the MSE.

For each of the four cases in Fig. 4, we separately discover closures for three elements of the SGS stress tensor. We also examine several LES grid sizes, and the effect of varying  $\alpha$ , which as mentioned earlier, is a key hyper-parameter in equation discovery. We use  $n = 100$  FDNS samples from a training set and 20 FDNS samples from an independent testing set. We evaluate the *a priori* performance using the commonly employed average correlation coefficient (CC), Eq. (5), on the test samples [2, 21, 71, 72].

As an illustrative example, Fig. 1(a) displays the mean CC for all elements of  $\tau_{ij}$  as  $\alpha$  increases. Note that this *structural modeling* approach is what all past equation-discovery studies followed [20, 21]. For small  $\alpha$  ( $< 1$ ), no closure is discovered (CC = 0, zero terms). As  $\alpha$  increases, the number of discovered terms increases, and the CC value rises and eventually plateaus, forming an “L-Curve.” The elbow of this curve is commonly used to identify the  $\alpha$  that balances accuracy and model size in equation discovery [20, 54, 59]. In Fig. 1(a), the CC- $\alpha$  relationship for each element of  $\tau_{ij}$  converges to approximately 1 and robustly discovers the same model at the elbow. Past studies [20, 21] found that the elbow of this curve (red circles) corresponds to the analytically derivable NGM2 [15, 16]. However, as these studies and earlier work found, LES with NGM2 leads to unstable *a posteriori* (online) simulations. Jakhar *et al.* [21]

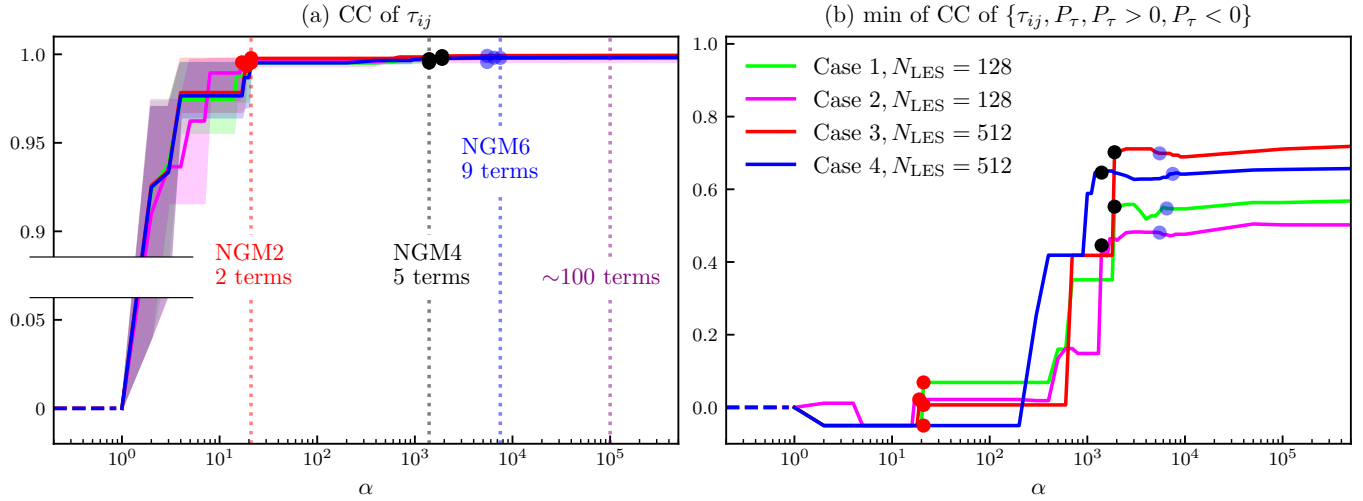


FIG. 1. Representative examples of the effects of increasing the sparsity-level hyperparameter,  $\alpha$ , on the CC in the discovered closure. (a)-(b) The CC- $\alpha$  relationship. In (a), the shading represents the max-min spread of all three elements of  $\tau_{ij}$ . (a) uses the common metric, CC of  $\tau_{ij}$ , while (b) uses a physics-informed metric that accounts for the CC of total ( $P_\tau$ ), diffusion ( $P_\tau > 0$ ), and backscattering ( $P_\tau < 0$ ) inter-scale energy transfers as well.

suggested that this instability is due to the inability of NGM2 in capturing any inter-scale energy transfers; i.e.,  $P_\tau^{\text{NGM2}}(x_1, x_2) = 0$  (NGM2 captures neither diffusion nor backscattering).

Here, we introduce a physics-informed discovery criterion that requires not only accurate reconstruction of  $\tau_{ij}$  but also capturing the inter-scale energy transfer (both diffusion and backscattering), thus combining structural and functional modeling. Figure 1(b) demonstrates that the L-curve in this new approach does not form an elbow around NGM2 (red circles), but rather, discovers a new closure (black circles) that has CC of  $\tau_{ij} > 0.99$  (Fig. 1(a)) and non-zero inter-scale energy transfer (Fig. 1(b)). We have found that the closure dis-

covered at the new elbow is NGM2 plus the second term from the Taylor-series expansion involving the higher orders ( $\mathcal{O}(\Delta^4)$ ), where filter width,  $\Delta$ , is twice the LES grid spacing (see Eq. (4)). We refer to this new closure as NGM4. As shown below, NGM4 outperforms existing physics-based closures in *a priori* and *a posteriori* tests.

It is noteworthy that the L-curves in Fig. 1 are consistently observed for all cases with any other  $N_{LES}$ . Note that increasing  $\alpha$  leads to another closure with more terms but negligible improvements in CC; we have found this closure to be NGM6; see Eq. (4) (a generalized Taylor-series expansion of  $\tau_{ij}$  is provided in the supplementary information [73]).

$$\tau_{ij}^{\text{NGM6}} = \underbrace{\frac{1}{1!} \frac{\Delta^2}{12} \left( \frac{\partial \bar{u}_i}{\partial x_k} \frac{\partial \bar{u}_j}{\partial x_k} \right)}_{\tau_{ij}^{\text{NGM2}}} + \underbrace{\frac{1}{2!} \frac{\Delta^4}{12^2} \left( \frac{\partial^2 \bar{u}_i}{\partial x_k \partial x_l} \frac{\partial^2 \bar{u}_j}{\partial x_k \partial x_l} \right)}_{\tau_{ij}^{\text{NGM4}}} + \frac{1}{3!} \frac{\Delta^6}{12^3} \left( \frac{\partial^3 \bar{u}_i}{\partial x_k \partial x_l \partial x_m} \frac{\partial^3 \bar{u}_j}{\partial x_k \partial x_l \partial x_m} \right) + \mathcal{O}(\Delta^8). \quad (4)$$

The equation discovery with the expansive 930-term library confirms that Taylor-series expansion offers the best representation of both  $\tau_{ij}$  and the inter-scale energy transfer. Note that the memory terms never emerged during the discovery.

We first compare the *a priori* (offline) performance of NGMs (NGM2-6) with common baseline closures, the eddy-viscosity Smagorinsky (Smag) [26], its dynamic version (DSmag) [23], and the dynamic Leith (DLeith) [25] models (see Appendix D). Figure 2 shows that NGM4

and NGM6 perfectly capture the structure of the FDNS SGS stress and inter-scale enstrophy transfers, and very well capture the inter-scale energy transfers (both diffusion and backscattering), significantly outperforming NGM2 and the physics-based closures.

An important feature of NGM4 and NGM6 is that they capture the energy backscatter that is seen in the FDNS. While the overall representations of inter-scale energy transfer of NGM4 and NGM6 are not perfect (around 62% and 78% of FDNS, respectively), they are substan-

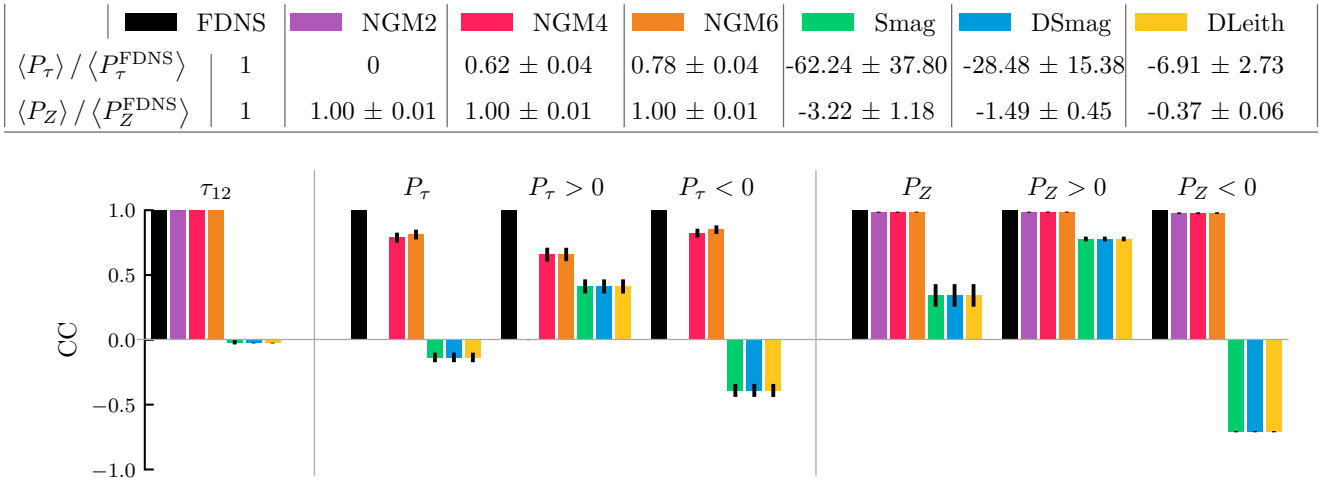


FIG. 2. Comparison of the *a priori* (offline) performance of different closures. The table shows the ratio of domain-averaged  $P_\tau$  and  $P_Z$  to that of FDNS. The bar plots present the CC for  $\tau_{12}$ ,  $P_\tau$ , and  $P_Z$  of each closure and FDNS. All values are the mean and standard deviations calculated for the 4 setups together (Cases 1-2 at  $N_{\text{LES}} = 128$  and Cases 3-4 at  $N_{\text{LES}} = 512$ ); Table S1 shows the values for each case.

tially better than the energy transfers of NGM2 ( $= 0$ ) and the eddy-viscosity closures, which are purely and excessively diffusive (as indicated by the negative CC values). The advantages of NGM4 and 6, especially over the eddy-viscosity closures, can also be seen in the inter-scale energy and enstrophy transfers' spectra (Fig. S1). These *a priori* tests show that NGM4 and NGM6 are fairly comparable, though NGM6 has a better  $P_\tau$  (see Table S1).

NGM4 and NGM6's strong *a priori* performance is reflected in their superior *a posteriori* performance. LES [74] with NGM4 and NGM6 remain long-term stable when the LES resolution is high enough to capture over 80% of DNS enstrophy (see Fig. S2). This is reminiscent of findings in 3D turbulence, where LES typically needs a resolution high enough to cover at least 80% of DNS kinetic energy [1].

In the atmosphere, intense cyclonic and anticyclonic vortices, which have positive and negative vorticity and are associated with low- and high-pressure systems, respectively, can drive various kinds of weather extremes [75]. Therefore, in this prototype of atmospheric turbulent circulation, the tails of the probability distribution function (PDF) of vorticity represent low-probability, rare “extreme weather” events. As shown in Figs. 3 and S3-S4, when stable, LES with NGM4 and NGM6 capture both the bulk and tails of the PDF of vorticity. LES with eddy-viscosity closures fail to capture the extremes, especially for Cases 3 and 4, which have high-wavenumber forcings. Note that using NGM2 for any case and any LES resolution leads to instabilities.

In addition to better capturing extreme events, LES with NGM4 and NGM6 outperforms eddy-viscosity models in short-term forecasting of vorticity (see insets of panels (a)-(b) in Figs. 3 and S3-S4).

LES with NGM4 and NGM6 also outperform LES with other closures in capturing the domain-averaged kinetic energy and enstrophy (Table S2). Figures 3, S3 (c)-(d), and S4 (b) show the enstrophy spectra of FDNS and LES. The insets magnifying the tails of the spectra do not clearly show the superiority of LES with any specific closure. However, the insets magnifying the spectra at lower wavenumbers reveal that LES with eddy-viscosity closures underestimate the enstrophy at large scales, likely due to the excessive diffusion. The same observation can be made about the energy spectra (Fig. S5). Note that in *a posteriori* tests, LES with NGM4 and NGM6 show fairly similar performances, suggesting that in practice, using NGM4 might be enough.

In conclusion, a physics-informed data-driven discovery identified an analytically derivable, yet previously ignored, representation of SGS closure that satisfies both *structural* and *functional* modeling requirements. This closure (NGM4) is “interpretable” as it is derivable from the Taylor-series expansion and it represents the Leonard and cross stresses (see supplementary information [73]). This closure is “generalizable” since its coefficients are entirely determined by the filter width ( $\Delta$ ) and does not have any component that depends on  $Re$  or any other parameters. NGM4 is accurate: it is the first closure to simultaneously excel in both *a priori* and *a posteriori* tests. LES with NGM4 is stable only when the numerical resolution is high enough to capture 80% of DNS enstrophy; however, this is consistent with general limitations of (explicit) LES [1] (see below for more discussions).

Although this closure could have been derived analytically decades ago, AI played a critical role in its discovery here. First, the analytical expansion of the gradient model to higher-order terms had not been previously pursued. Among the main reasons are that the source of the

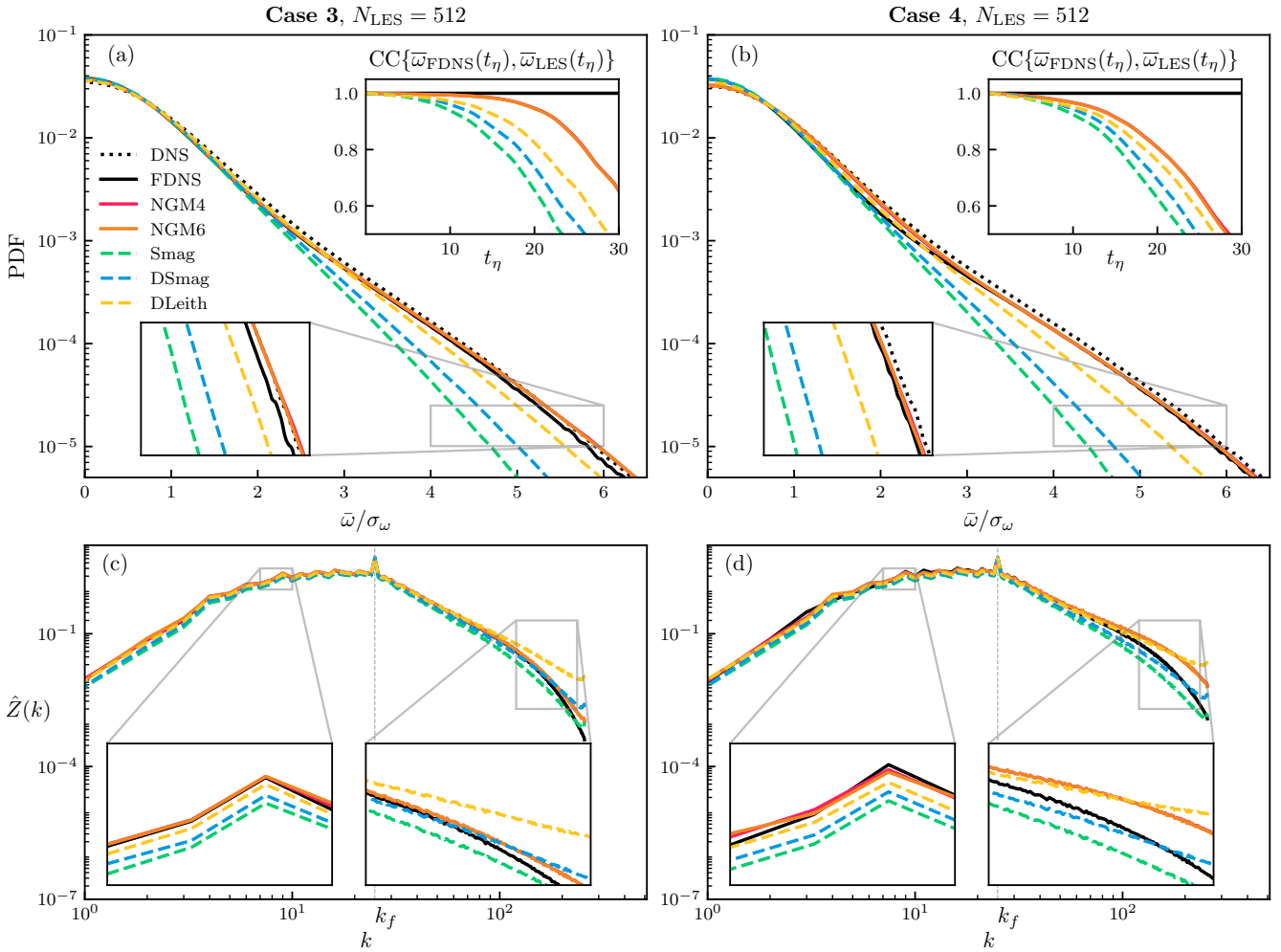


FIG. 3. Comparison of the *a posteriori* performance of different closures for Cases 3-4 at  $N_{LES} = 512$ . (a)-(b) The PDF of vorticity normalized by its standard deviation,  $\bar{\omega}/\sigma_\omega$ . The upper-right insets of (a)-(b) compares the accuracy of short-term forecasting of each LES against FDNS. The  $x$ -axis represents the eddy-turnover time,  $t_\eta = 1/\sqrt{\langle \bar{\omega}^2 \rangle}$ . (c)-(d) Comparison of the enstrophy spectra,  $\hat{Z}(k)$ , of LES with different closures. A similar figure for (Cases 1-2 at  $N_{LES} = 128$  and Case 4 at  $N_{LES} = 1024$ ) is shown in the supplementary information.

shortcoming of NGM2 was unclear and gradient closures were generally ignored in favor of stable eddy-viscosity ones. The sparse equation discovery showed that among 930 terms, NGM4 and NGM6 best represent both the stress tensor and inter-scale energy transfer. It was only after the AI-based discovery that the connection with higher-order Taylor-series expansion became clear.

A major difference between NGM4 and NGM6 is that the latter represents the Reynolds stress too (see supplementary information [73]). However, while *a priori* tests show that NGM6 better represents the inter-scale energy transfer, *a posteriori* tests do not demonstrate any advantage over NGM4 in terms of stability or accuracy. This is encouraging as implementing models with high-order derivatives in numerical solvers can be challenging; these findings suggest that NGM4 might suffice in practice, e.g., in ocean modeling. We note that NGM4

and NGM6 violate the Boussinesq hypothesis as they depend on second-order velocity gradients, highlighting the need to go beyond classical turbulence tensors to represent backscatter and anisotropic effects [64].

The findings of this work can also be framed within the broader context of nonlocal closures [76–80]. The finite-order gradient closures (Eq. (4)) can be viewed as truncations of the nonlocal deconvolution operator [2]. Therefore, NGM4 can be interpreted as the minimal local truncation that successfully captures the leading-order nonlocal effects required by our reconstruction and inter-scale transfer criteria. This interpretation suggests that for cases requiring stronger scale-selectivity or wider spectral fidelity, Padé-like rational approximations [81] or explicitly nonlocal kernels can be a natural extension.

Furthermore, we find that NGM4, a deterministic, local closure, suffices for these cases of 2D turbulence with

our chosen criteria. However, this still leaves the door open for stochastic (e.g., generative) extensions and closures with memory. In particular, applying equation-discovery methodologies to find parsimonious stochastic closures [82, 83] is therefore a promising direction for future work.

It is also important to note that in practice, many applications, such as weather and climate modeling, use “implicit” LES [84, 85]. In these highly under-resolved simulations, the numerical discretization acts as an implicit closure, effectively fusing the numerical method and the SGS modeling. Our work presents a testable, resolution-aware closure that, in the explicit LES regime, is compelling for its verified inter-scale energetics and *a posteriori* performance. In the under-resolved implicit LES regimes, this closure can serve as a target for diagnostics of inter-scale transfers and extremes, aid interpretability studies, and potentially be combined with existing discretization schemes when an explicit representation of backscatter is desired.

Finally, it should be noted that while here we only focused on the SGS stress tensor in 2D turbulence, these findings are relevant to multi-scale modeling in other dynamical systems too, as coarse-graining any quadratic nonlinearity can lead to an NGM-like representation, e.g., as already shown for heat flux in Rayleigh-Bénard convection [21]. This work also presents the importance of combining physical and mathematical insight to better

harness the power of AI methods in accelerating scientific discovery.

## Acknowledgment

We thank two anonymous reviewers for insightful feedback. This work is supported by NSF grant AGS-2046309 and Schmidt Sciences. Computational resources were provided by NSF ACCESS (allocation ATM170020) and NCAR’s CISL (allocation URIC0009).

## Data availability

The code for the numerical solver “py2d” is available at [74]. The codes and data for equation discovery and analysis in this work can be found at [86, 87].

## Author Contributions

All authors participated in conceptualizing the project, designing the computational experiments, and interpreting the results. K.J. developed the codes, performed the analysis, and generated the figures. P.H. acquired the funding and supervised the research.

---

[1] S. Pope, *Turbulent flows* (Cambridge university press, 2000).

[2] P. Sagaut, *Large eddy simulation for incompressible flows: an introduction* (Springer Science & Business Media, 2006).

[3] D. Randall, M. Khairoutdinov, A. Arakawa, and W. Grabowski, Breaking the cloud parameterization deadlock, *Bulletin of the American Meteorological Society* **84**, 1547 (2003).

[4] H. T. Hewitt, M. Roberts, P. Mathiot, A. Biastoch, E. Blockley, E. P. Chassignet, B. Fox-Kemper, P. Hyder, D. P. Marshall, E. Popova, *et al.*, Resolving and parameterising the ocean mesoscale in earth system models, *Current Climate Change Reports* **6**, 137 (2020).

[5] B. Fox-Kemper, A. Adcroft, C. W. Böning, E. P. Chassignet, E. Curchitser, G. Danabasoglu, C. Eden, M. H. England, R. Gerdes, R. J. Greatbatch, *et al.*, Challenges and prospects in ocean circulation models, *Frontiers in Marine Science* **6**, 65 (2019).

[6] C. Meneveau and J. Katz, Scale-invariance and turbulence models for large-eddy simulation, *Annual Review of Fluid Mechanics* **32**, 1 (2000).

[7] K. Duraisamy, G. Iaccarino, and H. Xiao, Turbulence modeling in the age of data, *Annual review of fluid mechanics* **51**, 357 (2019).

[8] T. Palmer, Climate forecasting: Build high-resolution global climate models, *Nature* **515**, 338 (2014).

[9] J. Slingo and T. Palmer, Uncertainty in weather and climate prediction, *Philosophical Transactions of the Royal Society A: Mathematical, Physical and Engineering Sciences* **369**, 4751 (2011).

[10] C.-Y. Lai, P. Hassanzadeh, A. Sheshadri, M. Sonnewald, R. Ferrari, and V. Balaji, Machine learning for climate physics and simulations, *Annual Review of Condensed Matter Physics* **16** (2024).

[11] A. Bracco, J. Brajard, H. A. Dijkstra, P. Hassanzadeh, C. Lessig, and C. Monteleoni, Machine learning for the physics of climate, *Nature Reviews Physics* **7**, 6 (2025).

[12] J. Berner, U. Achatz, L. Batte, L. Bengtsson, A. De La Camara, H. M. Christensen, M. Colangeli, D. R. Coleman, D. Crommelin, S. I. Dolaptchiev, *et al.*, Stochastic parameterization: Toward a new view of weather and climate models, *Bulletin of the American Meteorological Society* **98**, 565 (2017).

[13] P. Gentine, M. Pritchard, S. Rasp, G. Reinaudi, and G. Yacalis, Could machine learning break the convection parameterization deadlock?, *Geophysical Research Letters* **45**, 5742 (2018).

[14] J. Marston and S. Tobias, Recent developments in theories of inhomogeneous and anisotropic turbulence, *Annual Review of Fluid Mechanics* **55**, 351 (2023).

[15] A. Leonard, Energy cascade in large-eddy simulations of turbulent fluid flows, in *Advances in geophysics*, Vol. 18 (Elsevier, 1975) pp. 237–248.

[16] R. A. Clark, J. H. Ferziger, and W. C. Reynolds, Evaluation of subgrid-scale models using an accurately simulated turbulent flow, *Journal of fluid mechanics* **91**, 1 (1979).

[17] A. Leonard, Large-eddy simulation of chaotic convection and beyond, in *35th Aerospace Sciences Meeting and Exhibit* (1997) p. 204.

[18] D. Carati, S. Ghosal, and P. Moin, On the representation of backscatter in dynamic localization models, *Physics of Fluids* **7**, 606 (1995).

[19] G. L. Eyink, Multi-scale gradient expansion of the turbulent stress tensor, *Journal of Fluid Mechanics* **549**, 159 (2006).

[20] L. Zanna and T. Bolton, Data-driven equation discovery of ocean mesoscale closures, *Geophysical Research Letters* **47**, e2020GL088376 (2020).

[21] K. Jakhar, Y. Guan, R. Mojgani, A. Chattopadhyay, and P. Hassanzadeh, Learning closed-form equations for subgrid-scale closures from high-fidelity data: Promises and challenges, *Journal of Advances in Modeling Earth Systems* **16**, e2023MS003874 (2024).

[22] D. K. Lilly, The representation of small-scale turbulence in numerical simulation experiments, in *Proc. IBM Sci. Comput. Symp. on Environmental Science* (1967) pp. 195–210.

[23] M. Germano, U. Piomelli, P. Moin, and W. H. Cabot, A dynamic subgrid-scale eddy viscosity model, *Physics of Fluids A: Fluid Dynamics* **3**, 1760 (1991).

[24] D. K. Lilly, A proposed modification of the Germano subgrid-scale closure method, *Physics of Fluids A: Fluid Dynamics* **4**, 633 (1992).

[25] C. Leith, Stochastic models of chaotic systems, *Physica D: Nonlinear Phenomena* **98**, 481 (1996).

[26] J. Smagorinsky, General circulation experiments with the primitive equations: I. the basic experiment, *Monthly weather review* **91**, 99 (1963).

[27] G. Shutts, A kinetic energy backscatter algorithm for use in ensemble prediction systems, *Quarterly Journal of the Royal Meteorological Society: A journal of the atmospheric sciences, applied meteorology and physical oceanography* **131**, 3079 (2005).

[28] S. Chen, R. E. Ecke, G. L. Eyink, M. Rivera, M. Wan, and Z. Xiao, Physical mechanism of the two-dimensional inverse energy cascade, *Physical review letters* **96**, 084502 (2006).

[29] M. F. Jansen and I. M. Held, Parameterizing subgrid-scale eddy effects using energetically consistent backscatter, *Ocean Modelling* **80**, 36 (2014).

[30] M. F. Jansen, I. M. Held, A. Adcroft, and R. Hallberg, Energy budget-based backscatter in an eddy permitting primitive equation model, *Ocean Modelling* **94**, 15 (2015).

[31] I. Grooms, Y. Lee, and A. J. Majda, Numerical schemes for stochastic backscatter in the inverse cascade of quasi-geostrophic turbulence, *Multiscale Modeling & Simulation* **13**, 1001 (2015).

[32] S. Khani and M. L. Waite, Backscatter in stratified turbulence, *European Journal of Mechanics-B/Fluids* **60**, 1 (2016).

[33] A. Ross, Z. Li, P. Perezhogin, C. Fernandez-Granda, and L. Zanna, Benchmarking of machine learning ocean subgrid parameterizations in an idealized model, *Journal of Advances in Modeling Earth Systems* **15**, e2022MS003258 (2023).

[34] S. Khani and C. N. Dawson, A gradient based subgrid-scale parameterization for ocean mesoscale eddies, *Journal of Advances in Modeling Earth Systems* **15**, e2022MS003356 (2023).

[35] M. Kang, Y. Jeon, and D. You, Neural-network-based mixed subgrid-scale model for turbulent flow, *Journal of Fluid Mechanics* **962**, A38 (2023).

[36] P. Perezhogin, C. Zhang, A. Adcroft, C. Fernandez-Granda, and L. Zanna, A stable implementation of a data-driven scale-aware mesoscale parameterization, *Journal of Advances in Modeling Earth Systems* **16**, e2023MS004104 (2024).

[37] Y. Guan, A. Chattopadhyay, A. Subel, and P. Hassanzadeh, Stable a posteriori LES of 2D turbulence using convolutional neural networks: Backscattering analysis and generalization to higher Re via transfer learning, *Journal of Computational Physics* **458**, 111090 (2022).

[38] Y. Guan, P. Hassanzadeh, T. Schneider, O. Dunbar, D. Z. Huang, J. Wu, and I. Lopez-Gomez, Online learning of eddy-viscosity and backscattering closures for geophysical turbulence using ensemble kalman inversion, *arXiv preprint arXiv:2409.04985* (2024).

[39] D. Carati, G. S. Winckelmans, and H. Jeanmart, On the modelling of the subgrid-scale and filtered-scale stress tensors in large-eddy simulation, *Journal of Fluid Mechanics* **441**, 119 (2001).

[40] R. D. Moser, S. W. Haering, and G. R. Yalla, Statistical properties of subgrid-scale turbulence models, *Annual Review of Fluid Mechanics* **53**, 255 (2021).

[41] S. L. Brunton, B. R. Noack, and P. Koumoutsakos, Machine learning for fluid mechanics, *Annual review of fluid mechanics* **52**, 477 (2020).

[42] V. Eyring, W. D. Collins, P. Gentine, E. A. Barnes, M. Barreiro, T. Beucler, M. Bocquet, C. S. Bretherton, H. M. Christensen, K. Dagon, *et al.*, Pushing the frontiers in climate modelling and analysis with machine learning, *Nature Climate Change* **14**, 916 (2024).

[43] R. Maulik, O. San, A. Rasheed, and P. Vedula, Data-driven deconvolution for large eddy simulations of Kraichnan turbulence, *Physics of Fluids* **30**, 125109 (2018).

[44] A. Beck, D. Flad, and C.-D. Munz, Deep neural networks for data-driven LES closure models, *Journal of Computational Physics* **398**, 108910 (2019).

[45] A. Subel, Y. Guan, A. Chattopadhyay, and P. Hassanzadeh, Explaining the physics of transfer learning in data-driven turbulence modeling, *PNAS Nexus*, pgad015 (2023).

[46] K. Srinivasan, M. D. Chekroun, and J. C. McWilliams, Turbulence closure with small, local neural networks: Forced two-dimensional and  $\beta$ -plane flows, *Journal of Advances in Modeling Earth Systems* **16**, e2023MS003795 (2024).

[47] G. Novati, H. L. de Laroussilhe, and P. Koumoutsakos, Automating turbulence modelling by multi-agent reinforcement learning, *Nature Machine Intelligence* **3**, 87 (2021).

[48] H. J. Bae and P. Koumoutsakos, Scientific multi-agent reinforcement learning for wall-models of turbulent flows, *Nature Communications* **13**, 1443 (2022).

[49] M. Kurz, P. Offenhäuser, and A. Beck, Deep reinforcement learning for turbulence modeling in large eddy simulations, *International journal of heat and fluid flow* **99**, 109094 (2023).

[50] C. Wang, J. Berner, Z. Li, D. Zhou, J. Wang, J. Bae, and A. Anandkumar, Coarse graining with neural operators for simulating chaotic systems, *arXiv preprint arXiv:2408.05177* (2025).

[51] M. Schmidt and H. Lipson, Distilling free-form natural laws from experimental data, *science* **324**, 81 (2009).

[52] S.-M. Udrescu and M. Tegmark, Ai Feynman: A physics-inspired method for symbolic regression, *Science Advances* **6**, eaay2631 (2020).

[53] S. L. Brunton, J. L. Proctor, and J. N. Kutz, Discovering governing equations from data by sparse identification of nonlinear dynamical systems, *Proceedings of the national academy of sciences* **113**, 3932 (2016).

[54] S. Zhang and G. Lin, Robust data-driven discovery of governing physical laws with error bars, *Proceedings of the Royal Society A: Mathematical, Physical and Engineering Sciences* **474**, 20180305 (2018).

[55] Y. Chen, Y. Luo, Q. Liu, H. Xu, and D. Zhang, Symbolic genetic algorithm for discovering open-form partial differential equations (SGA-PDE), *Physical Review Research* **4**, 023174 (2022).

[56] A. Grundner, T. Beucler, P. Gentine, and V. Eyring, Data-driven equation discovery of a cloud cover parameterization, *Journal of Advances in Modeling Earth Systems* **16**, e2023MS003763 (2024).

[57] J. Newey, J. P. Whitehead, and E. Carlson, Model discovery on the fly using continuous data assimilation, *Journal of Computational Physics* , 114121 (2025).

[58] M. Cranmer, Interpretable machine learning for science with PySR and SymbolicRegression. jl, arXiv preprint arXiv:2305.01582 (2023).

[59] R. Mojgani, A. Chattopadhyay, and P. Hassanzadeh, Discovery of interpretable structural model errors by combining Bayesian sparse regression and data assimilation: A chaotic Kuramoto-Sivashinsky test case, *Chaos: An Interdisciplinary Journal of Nonlinear Science* **32**, 061105 (2022).

[60] M. E. Tipping, Sparse Bayesian learning and the relevance vector machine, *Journal of machine learning research* **1**, 211 (2001).

[61] J. Wouters and V. Lucarini, Multi-level dynamical systems: Connecting the ruelle response theory and the mori-zwanzig approach, *Journal of Statistical Physics* **151**, 850 (2013).

[62] E. J. Parish and K. Duraisamy, Non-markovian closure models for large eddy simulations using the mori-zwanzig formalism, *Physical Review Fluids* **2**, 014604 (2017).

[63] K. Jakhar, Arbfft: Arbitrary precision fast fourier transform in python (version 1.0) (2024).

[64] S. Pope, A more general effective-viscosity hypothesis, *Journal of Fluid Mechanics* **72**, 331 (1975).

[65] J. A. Anstey and L. Zanna, A deformation-based parametrization of ocean mesoscale eddy Reynolds stresses, *Ocean Modelling* **112**, 99 (2017).

[66] T. B. Gatski and C. G. Speziale, On explicit algebraic stress models for complex turbulent flows, *Journal of fluid Mechanics* **254**, 59 (1993).

[67] T. Jongen and T. Gatski, General explicit algebraic stress relations and best approximation for three-dimensional flows, *International Journal of Engineering Science* **36**, 739 (1998).

[68] T. S. Lund and E. Novikov, Parameterization of subgrid-scale stress by the velocity gradient tensor, *Annual Research Briefs*, 1992 (1993).

[69] H. Li, Y. Zhao, J. Wang, and R. D. Sandberg, Data-driven model development for large-eddy simulation of turbulence using gene-expression programing, *Physics of Fluids* **33**, 125127 (2021).

[70] M. Reissmann, J. Hasslberger, R. D. Sandberg, and M. Klein, Application of gene expression programming to a-posteriori LES modeling of a Taylor Green vortex, *Journal of Computational Physics* **424**, 109859 (2021).

[71] R. Maulik, O. San, A. Rasheed, and P. Vedula, Subgrid modelling for two-dimensional turbulence using neural networks, *Journal of Fluid Mechanics* **858**, 122 (2019).

[72] Y. Guan, A. Subel, A. Chattopadhyay, and P. Hassanzadeh, Learning physics-constrained subgrid-scale closures in the small-data regime for stable and accurate LES, *Physica D: Nonlinear Phenomena* **443**, 133568 (2023).

[73] See Supplemental Material at [URL] for additional figures, tables, and methodological details, which includes [88–91].

[74] K. Jakhar, R. Mojgani, M. Darman, Y. Guan, and P. Hassanzadeh, py2d: High-performance 2D Navier-Stokes solver in python (version 0.1) (URL:<https://github.com/envfluids/py2d>) (2024).

[75] G. K. Vallis, *Atmospheric and oceanic fluid dynamics* (Cambridge University Press, 2017).

[76] J. Philip, Diffusion by continuous movements, *The Physics of Fluids* **11**, 38 (1968).

[77] E. Knobloch, The diffusion of scalar and vector fields by homogeneous stationary turbulence, *Journal of Fluid Mechanics* **83**, 129 (1977).

[78] F. Hamba, Analysis and modelling of non-local eddy diffusivity for turbulent scalar flux, *Journal of Fluid Mechanics* **950**, A38 (2022).

[79] Y. Shirian and A. Mani, Eddy diffusivity operator in homogeneous isotropic turbulence, *Physical Review Fluids* **7**, L052601 (2022).

[80] E. Villermaux, The nonlocal nature of the reynolds stress, *Comptes Rendus. Mécanique* **353**, 879 (2025).

[81] T. Iliescu and P. F. Fischer, Large eddy simulation of turbulent channel flows by the rational large eddy simulation model, *Physics of Fluids* **15**, 3036 (2003).

[82] T. Schneider, A. M. Stuart, and J.-L. Wu, Learning stochastic closures using ensemble Kalman inversion, *Transactions of Mathematics and Its Applications* **5**, tnab003 (2021).

[83] X. Dong, H. Yang, and J.-L. Wu, Stochastic and non-local closure modeling for nonlinear dynamical systems via latent score-based generative models, arXiv preprint arXiv:2506.20771 (2025).

[84] L. G. Margolin, W. J. Rider, and F. F. Grinstein, Modeling turbulent flow with implicit les, *Journal of Turbulence* , N15 (2006).

[85] K. G. Pressel, S. Mishra, T. Schneider, C. M. Kaul, and Z. Tan, Numerics and subgrid-scale modeling in large eddy simulations of stratocumulus clouds, *Journal of advances in modeling earth systems* **9**, 1342 (2017).

[86] K. Jakhar, Equation discovery for 2d turbulence (URL:[https://github.com/jakharkaran/EqsDiscovery\\_2DTurbulence](https://github.com/jakharkaran/EqsDiscovery_2DTurbulence)).

[87] K. Jakhar, Y. Guan, and P. Hassanzadeh, Dataset: An analytical and ai-discovered stable, accurate, and generalizable subgrid-scale closure for geophysical turbulence (2025).

[88] M. Rivera, W. Daniel, S. Chen, and R. E. Ecke, Energy and enstrophy transfer in decaying two-dimensional turbulence, *Physical review letters* **90**, 104502 (2003).

[89] S. Chen, R. E. Ecke, G. L. Eyink, X. Wang, and Z. Xiao, Physical mechanism of the two-dimensional enstrophy

cascade, *Physical review letters* **91**, 214501 (2003).

[90] C. G. Speziale, Galilean invariance of subgrid-scale stress models in the large-eddy simulation of turbulence, *Journal of fluid mechanics* **156**, 55 (1985).

[91] M. Germano, A proposal for a redefinition of the turbulent stresses in the filtered Navier-Stokes equations, *The Physics of fluids* **29**, 2323 (1986).

## END MATTER

*Appendix A:* Figure 4 shows the cases considered in this study and their physical and numerical parameters.

*Appendix B:* Correlation coefficient (CC) compares the 2D pattern of the “true” SGS stress,  $\tau^{\text{FDNS}}$  (from FDNS), with the predicted stress,  $\tau^{\text{RVM}}$ , which is generated by the RVM-discovered closure based on the filtered flow variables (e.g.,  $\bar{u}_1$ ,  $\bar{u}_2$ ) as input:

$$\text{CC} = \frac{\langle (\tau^{\text{RVM}} - \langle \tau^{\text{RVM}} \rangle) (\tau^{\text{FDNS}} - \langle \tau^{\text{FDNS}} \rangle) \rangle}{\sqrt{\langle (\tau^{\text{RVM}} - \langle \tau^{\text{RVM}} \rangle)^2 \rangle} \sqrt{\langle (\tau^{\text{FDNS}} - \langle \tau^{\text{FDNS}} \rangle)^2 \rangle}}, \quad (5)$$

where  $\langle \cdot \rangle$  is domain averaging.

*Appendix C:* The DNS/LES numerical solver is the same as the one used in [21, 37]. Briefly, the Navier-Stokes equations in the vorticity-streamfunction formulation, e.g., curl of Eq. (2) for LES, are solved

in a doubly periodic domain using a Fourier-Fourier pseudo-spectral solver. For time integration, we employ second-order Adams-Bashforth and Crank-Nicolson schemes for the advection and viscous terms, respectively.

*Appendix D:* The baseline physics-based closures used here are Smag, DSmag, and DLeith. These eddy viscosity closures introduce dissipation and do not account for backscattering:  $\tau_{ij} = -2\nu_e \bar{S}_{ij}$ , with  $\bar{S}_{ij}$  representing the filtered rate of strain and  $\nu_e$  denoting the eddy viscosity [1].  $\nu_e = (C_s \Delta)^2 \sqrt{2\bar{S}_{ij} \bar{S}_{ij}}$  for Smag and  $\nu_e = (C_l \Delta)^3 |\nabla \bar{\omega}|$  for Leith. We use  $C_s = 0.17$  for Smag, as proposed in a previous work [22];  $C_s$  and  $C_l$  are estimated dynamically based on the local flow structure for DSmag and DLeith, respectively. This procedure can yield  $\nu_e \leq 0$ , potentially resulting in numerical instabilities; therefore, the commonly used “positive clipping” is applied to enforce diffusion ( $\nu_e \geq 0$ ) [71].

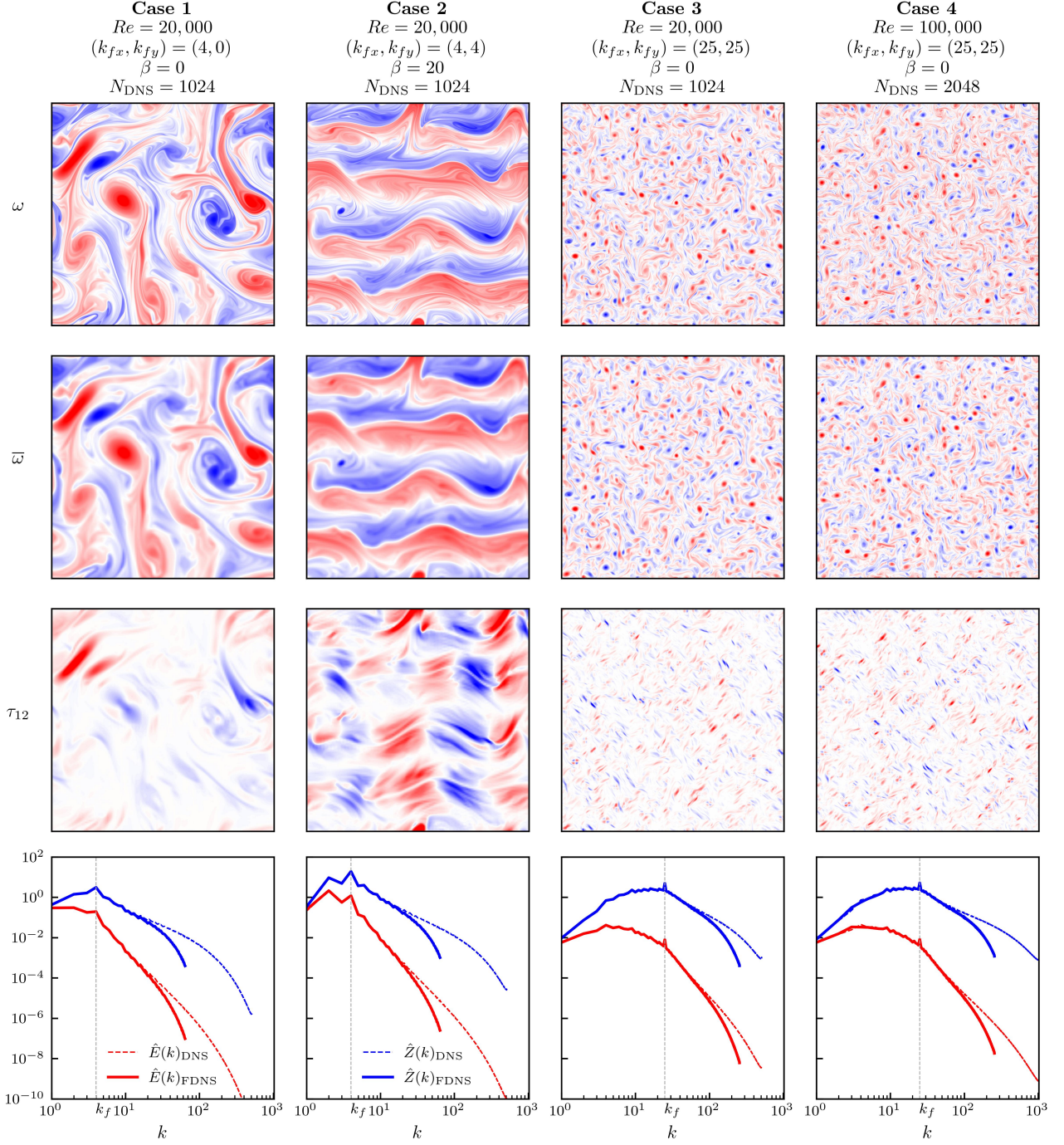


FIG. 4. The four cases considered in this study. These cases represent a broad range of dynamics in 2D turbulence and mimic the diversity of flow regimes (jets and vortices) in the atmosphere and ocean.  $(k_x, k_y)$  are the wavenumbers of the time-invariant forcing in the  $x$  and  $y$  directions, where higher wavenumbers lead to small-scale vortices and double cascade.  $\beta$  is the gradient of the Coriolis force, mimicking the effects of Earth's rotation and leading to the formation of jets (see [21] for more details about the dynamics of these cases).  $N_{\text{DNS}}$  is the resolution of the pseudo-spectral solver (in each direction) used for DNS (Jakhar *et al.* [74]). The first row presents snapshots of the DNS vorticity,  $\omega$ . The second row shows snapshots of the FDNS vorticity,  $\bar{\omega}$ . The third row displays a snapshot of an element of the SGS stress term,  $\tau_{12}$  (the subject of closure modeling). The last row depicts the energy (red line) and enstrophy (blue line) spectra for DNS (dashed line) and FDNS (solid line). FDNS is at  $N_{\text{LES}} = 128$  for Cases 1-2 and  $N_{\text{LES}} = 512$  for Cases 3-4.